Available online at www.sciencedirect.com
SCIENCE DIRECT
Earth and Planetary Science Letters 248 (2006) 54–61
EPSL
www.elsevier.com/locate/epsl

Mechanisms of Al^{3+} incorporation in $MgSiO_3$ post-perovskite at high pressures

Feiwu Zhang *, Artem R. Oganov

Laboratory of Crystallography, Department of Materials, ETH Zurich Wolfgang-Pauli-Strasse 10, CH-8093 Zurich, Switzerland

Received 17 February 2006; received in revised form 4 May 2006; accepted 14 May 2006
Available online 30 June 2006
Editor: G.D. Price

Abstract

Aluminum is the fifth most abundant element in the Earth's mantle, yet its effect on the physical properties of the newly found $MgSiO_3$ post-perovskite (*PPv*), the major mineral of the Earth's D″ layer, is not fully known. In this paper, large-scale *ab initio* simulations based on density functional theory (DFT) within the generalized gradient approximation (GGA) have been carried out in order to investigate the substitution mechanism of Al^{3+} into *PPv* at high pressures. We have examined three types of Al substitution in *PPv*: 6.25 mol% Al substitution via a charge-coupled mechanism (CCM), 6.25 mol% Al substitution via oxygen-vacancy mechanism (OVM), and an oxygen-vacancy Si-free end member $Mg_2Al_2O_5$. For both the CCM and OVM, five models, where the Al atoms were put in different positions, were simulated at various pressures in the range 10–150 GPa. Our calculations show that the most favorable mechanism is a charge-coupled substitution where Al^{3+} replaces the next-nearest-neighbor cation pairs in the *PPv* structure. The calculated zero-pressure bulk modulus of Al-bearing *PPv* is 3.15% lower than that of the Al-free *PPv*. In agreement with previous works, we find that the incorporation of Al_2O_3 slightly increases the post-perovskite phase transition pressure, with the Al partition coefficient $K=2.67$ at 120 GPa and 3000 K.

Keywords: $MgSiO_3$ post-perovskite; compressibility; equation of state; substitution mechanism; D″ layer; *ab initio*

1. Introduction

Seismic studies [1–6] have shown that the region above the CMB, called the D″ layer, contains strong seismic anomalies (e.g. seismic discontinuity, anisotropy, and an anticorrelation between the shear and bulk sound velocities). From the viewpoint of mineralogy and petrology, the Earth's lower mantle is believed to be composed mainly of Fe- and Al-bearing *Pv*, with about 4–6 mol% Fe and 4–6 mol% Al [7,8]. Recent experiments and theoretical calculations have shown that $MgSiO_3$ [9–11], Fe_2O_3 [12] and Al_2O_3 [13–16] will undergo a phase transition to the post-perovskite structure under lower mantle conditions, making $MgSiO_3$ post-perovskite (*PPv*) the main mineral phase of the D″ layer. Several studies [17–19] concluded that the incorporation of Al^{3+} into $MgSiO_3$ would increase the *Pv*–*PPv* transition pressure and, due to strong fractionation of Al^{3+} between *Pv* and *PPv*, will lead to a coexistence of *Pv* and *PPv* over a range of pressures. Puzzlingly, Akber-Knutson et al. [17] predicted this

* Corresponding author.
E-mail address: feiwu.zhang@mat.ethz.ch (F. Zhang).

0012-821X/$ - see front matter © 2006 Elsevier B.V. All rights reserved.
doi:10.1016/j.epsl.2006.05.015

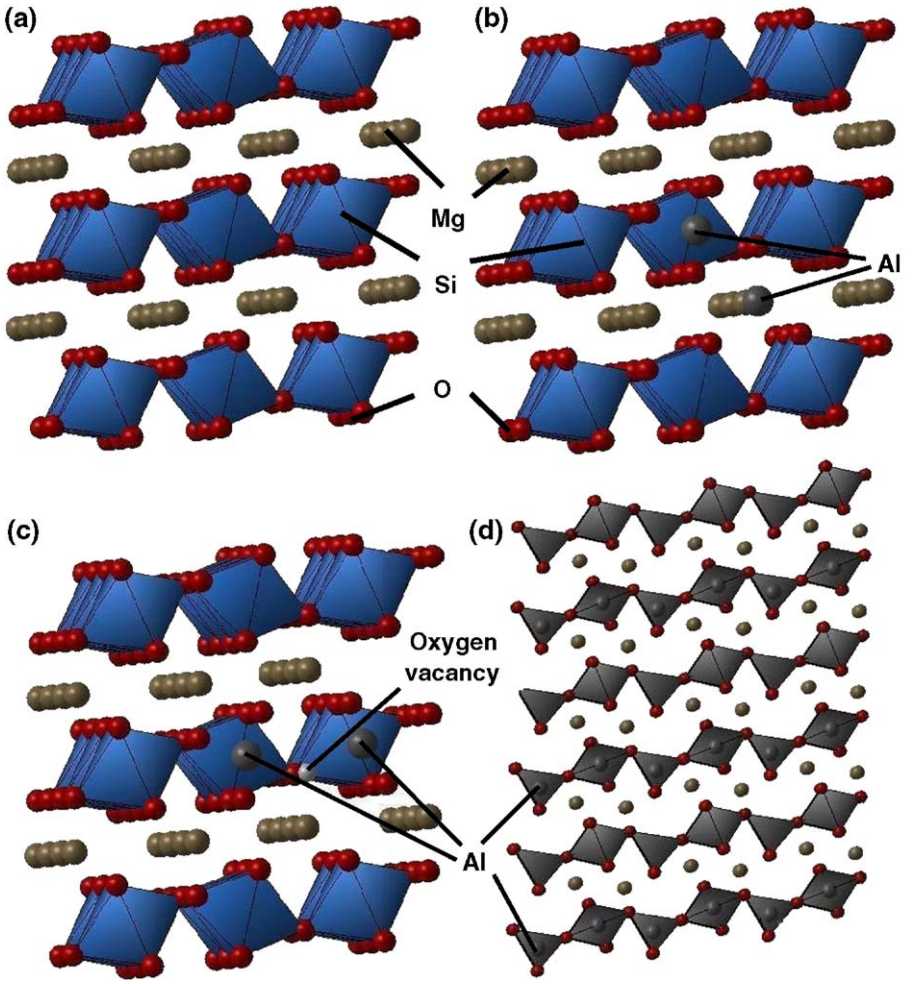

Fig. 1. Calculated structures: pure $MgSiO_3$–*PPv* (a), CCM (b), OVM (c) and the $Mg_2Al_2O_5$–*PPv* structure (d).

coexistence interval to be so large that the discontinuity due to the *Pv*–*PPv* transition could become seismically unobservable. Perhaps, this paradox can be resolved by considering coupled Fe^{3+}–Al^{3+} substitutions. Our previous simulations [20] showed that the main impurities, Al^{3+} and Fe^{3+}, enter the *PPv* structure independently of

Table 1
Fractional atomic positions of substituted Al in 160-atom *PPv* supercells at 100 GPa

	$Mg^{2+}\rightarrow Al^{3+}$	$Si^{4+}\rightarrow Al^{3+}$	*d* (Al–Al) Å	*V* (Å^3)	
CCM1	(0.575, 0.365, 0.461)	(0.512, 0.486, 0.271)	2.57	1019.85	
CCM2	(0.575, 0.365, 0.461)	(0.512, 0.236, 0.773)	2.80	1019.85	
CCM3	(0.575, 0.361, 0.463)	(0.262, 0.485, 0.523)	3.60	1019.86	
CCM4	(0.576, 0.360, 0.464)	(0.013, 0.236, 0.273)	4.53	1019.92	
CCM5	(0.576, 0.360, 0.464)	(0.263, 0.986, 0.523)	5.67	1020.08	
	$Si^{4+}\rightarrow Al^{3+}$	$Si^{4+}\rightarrow Al^{3+}$	Oxygen vacancy	*d* (Al–Al) Å	*V* (Å^3)
OVM1	(0.262, 0.486, 0.523)	(0.262, 0.236, 0.523)	(0.244, 0.361, 0.468)	3.19	1020.35
OVM2	(0.262, 0.486, 0.523)	(0.512, 0.486, 0.273)	(0.353, 0.515, 0.297)	3.19	1020.65
OVM3	(0.262, 0.486, 0.523)	(0.012, 0.736, 0.273)	(0.244, 0.361, 0.468)	4.51	1021.60
OVM4	(0.262, 0.486, 0.523)	(0.012, 0.736, 0.273)	(0.353, 0.515, 0.297)	4.51	1021.17
OVM5	(0.262, 0.486, 0.523)	(0.012, 0.736, 0.273)	(0.421, 0.456, 0.499)	4.51	1021.28

The substitution sites were chosen by the distance of Al–Al.

each other, forming separate [Al^{3+}–Al^{3+}] and [Fe^{3+}–Fe^{3+}] cation pairs. This is quite different from the preferred [Fe^{3+}–Al^{3+}] substitution in the $MgSiO_3$ perovskite phase (*Pv*) [21–23] and allows one to separate the effects of Al^{3+} and Fe^{3+} on properties of *PPv*.

Akber-Knutson et al. [17] found that CCM is more favorable than OVM. They showed that while both 6.25 and 100 mol% substitution of *PPv* by Al_2O_3 via a CCM, causes the zero-pressure volume (V_0) to decrease, the bulk modulus (K_0) increases by 1.5% in the former case, but decreases by 1.5% in the latter. This is opposite to the results of Caracas and Cohen [18], whose GGA calculations showed that 100 % substitution of *PPv* by Al_2O_3 causes both V_0 and K_0 to increase, and LDA calculations showed it to cause V_0 to increase and K_0 to decrease. The Al substitution configuration adopted by Akber-Knutson et al. [17] is not clear, although they stated that several configurations were considered in they work. Here, using large-scale *ab initio* simulations, we performed a systematic study of the substitution mechanism of Al^{3+} into *PPv* and the effects of Al^{3+} on its physical properties using state-of-the-art computational methods. The aim of our study is to clarify the microscopic details of the Al^{3+} substitution in *PPv*.

2. Computational methodology

Computations were performed using density functional theory (DFT) as implemented in the VASP code [24], within the generalized gradient approximation (GGA) [25] for electron exchange-correlation. To treat the interactions between the valence electrons and the core, the projector augmented wave (PAW) [26,27] method was used, which is a frozen-core all-electron approach where the exact valence wavefunction is used as opposed to the traditional pseudopotential methods, used by Akber-Knutson et al. [17]. In all calculations, the core region cut-off was 2.2 a.u. for Al (core configuration $1s^2 2s^2 2p^6 3s^2$), 2.0 a.u. for Mg (core configuration $1s^2 2s^2$), 1.5 a.u. for Si (core configuration $1s^2 2s^2 2p^6$), 1.52 a.u. for O (core configuration $1s^2$). For all calculations we used a 160-atom large supercell (see below), plane-wave cut-off of 500 eV and only the Γ-point was used for the Brillouin zone sampling. The basis set incompleteness errors are within 0.004 meV/atom for the total energy and 0.1 GPa for the compressional stresses, 0.5 GPa for the shear stresses, respectively. Structural relaxation was done using the conjugate-gradients method, until the total energy changes were below 10^{-4} eV.

In our calculations, two Al^{3+} ions (6.25 mol% of Al^{3+}) were put in the 160-atom *PPv* supercells (Fig. 1a–c) with the charge-coupled mechanism (CCM) $Al^{3+} \rightarrow Al^{\bullet}_{Mg} + Al'_{Si}$ [28,29], where $\bullet$ and $'$ superscripts represent a positive or negative net charge on the site, respectively. An alternative, the oxygen-vacancy mechanism (OVM) $2Al^{3+} \rightarrow 2Si^{4+} + O^{2-}$, was also considered. Here, we performed calculations using the same 160-atom *PPv* supercell where two adjacent Si^{4+} ions are both replaced by Al^{3+} ions, and the O^{2-} ion between them is removed to maintain charge balance. Such calculations were performed for the whole range of lower mantle pressures, at which all the atomic positions and cell parameters were allowed to relax at static conditions (0 K). In order to determine which atomic configuration for Al-incorporation through OVM and CCM is energetically favorable, we calculated five different CCMs and five different OVMs changing their atomic configuration. Earlier, Brodholt considered [28] Si-free oxygen-vacancy end-member $Mg_2Al_2O_5$ based on the *Pv* structure and made by the substitution of all Si atoms with Al and the removal of one in six oxygens from the normal *Pv* structure. We simulated a similar end-member for *PPv* also with the composition $Mg_2Al_2O_5$ (Fig. 1d).

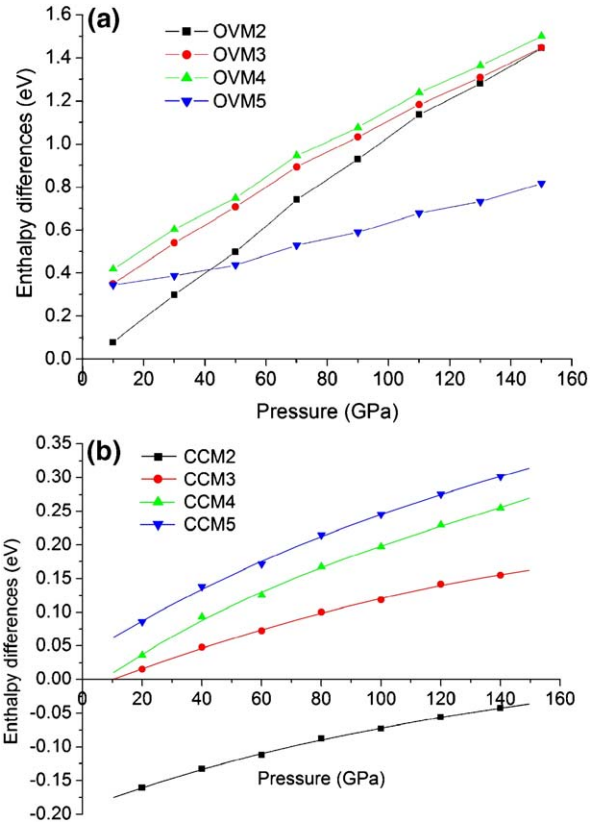

Fig. 2. Enthalpy differences of Al-incorporated models for (a) OVM and (b) CCM as functions of pressures relative to (a) OVM1 and (b) CCM1, respectively.

Table 2
Calculated Equation of State (EOS) parameters for all defect post-perovskites, pure $MgSiO_3$ post-perovskite and MgO

	V_0 (Å^3, 0 GPa)	K_0 (GPa)	K_0'	
[$MgSiO_3$]*PPv*	167.50	204.99	4.20	GGA (this work)[a]
	167.64	199.96	4.54	GGA[b]
	162.86	231.93	4.43	LDA[b]
	167.32	204	4.18	Theory[c]
$Mg_2Al_2O_5$	187.67	132.09	3.96	GGA (this work)[a]
MgO	76.96	152.6	4.08	GGA (this work)[a]
	76.2	168.7	4.26	Theory[d]
	74.7	160.2	3.99	Expt.[e]
CCM1	167.88	200.64	4.26	GGA (this work)[a]
CCM2	167.99	198.53	4.31	
CCM3	167.98	198.72	4.31	
CCM4	167.96	199.36	4.29	
CCM5	168.01	198.54	4.31	
CCM (12.5 mol% Al^{3+})	167.16	207	4.13	Theory[c]
CCM (100 mol% Al^{3+})	167.12	201	4.29	
OVM1	168.35	200.29	4.20	GGA (this work)[a]
OVM2	168.57	197.66	4.24	
OVM3	168.72	198.55	4.21	
OVM4	168.82	196.31	4.25	
OVM5	168.78	196.90	4.24	

[a] Third-order Birch–Murnaghan equation of state at 0 K.
[b] Vinet equation of state at 0 K [10].
[c] Theoretical third-order Birch–Murnaghan equation of state at 0 K [17].
[d] Theoretical Vinet equation of state at 0 K [31].
[e] Third-order birch–Murnaghan equation of state at 300 K [32].

Previous simulations by Akber-Knutson et al. [17] examined several atomic configurations of CCM and OVM with a very high Al_2O_3 concentration: 6.25 mol% (12.5 mol% of Al^{3+}) and 100 mol% of Al_2O_3. Table 1 lists all the fractional atomic positions of substituted Al atoms in $MgSiO_3$–*PPv* at 100 GPa. The substitution sites were chosen by the distance of Al–Al. Fig. 1 shows the calculated supercells of $MgSiO_3$–*PPv* (Al-free and two models of aluminous post-perovskite by CCM and OVM) and the $Mg_2Al_2O_5$–*PPv* structure. The cell vectors of that supercell are obtained from the cell vectors of the standard *Cmcm* cell through the transformation matrix: $M = \begin{pmatrix} 4 & 0 & 0 \\ 0 & 2 & 0 \\ 2 & 0 & 1 \end{pmatrix}$; the origin of the coordinate system has been shifted in the supercell by (1/4, 0, 0) after the transformation.

3. Results

The enthalpy differences of all calculated OVMs and CCMs relative to OVM1 or CCM1 are shown in Fig. 2a and b, respectively. At all the lower mantle pressures up to 150 GPa, model OVM1 is more favorable than other OVM models, and model CCM2 is more stable than other CCM models.

Table 2 shows the calculated parameters of the third-order Birch–Murnaghan equation of state (EOS) for all defect post-perovskites, together with those for pure $MgSiO_3$–*PPv* and MgO. Difference with previous work [17] on the effect of Al^{3+} substitution in *PPv* probably comes from the different atomic potentials PAW *vs.* pseudopotentials and the different

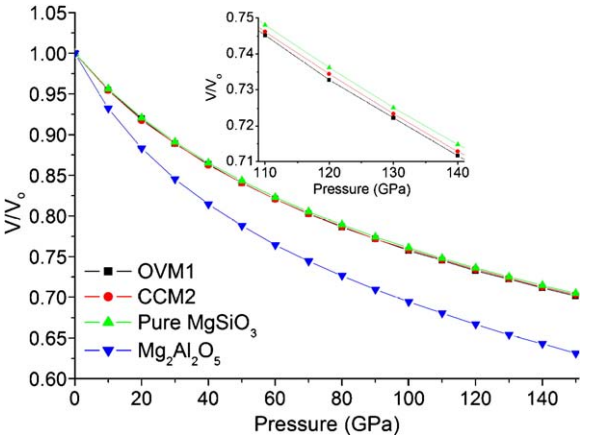

Fig. 3. Compressibility (V/V_0) of the three defect end-member post-perovskites together with pure $MgSiO_3$–*PPv*. The insert is for better visualization of V/V_0 between 110 and 140 GPa.

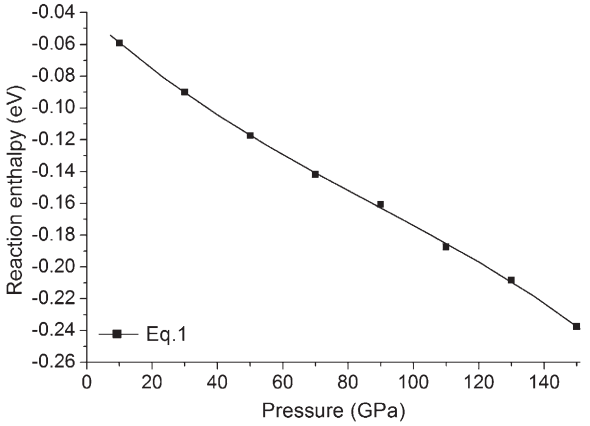

Fig. 4. Calculated enthalpy difference, ΔH, for the reaction in Eq. (1) as a function of pressure. Negative values indicate CCM is more energetically favorable.

optimization methods used in the simulations. Fig. 3 shows the compressibility of the three defect end-member post-perovskites together with that of pure $MgSiO_3$–*PPv*. The Al–Al substituted CCM2 model has a compressibility that is only slightly greater than that of the pure *PPv*. The significantly greater compressibility of $Mg_2Al_2O_5$ shows that, when present, oxygen vacancies will produce a strong increase in the compressibility of alumina-rich *PPv*, as in *Pv* [30].

To evaluate the stability of Al^{3+} incorporation into $MgSiO_3$ post-perovskite, we have considered several reactions (at fixed $x=6.25\%$):

$$\mathrm{Mg(Si_{1-x}A1_x)O_{3-x/2}} + x/2\mathrm{MgSiO_3} \rightarrow (\mathrm{Mg_{1-x/2}Al_{x/2}}) \times (\mathrm{Si_{1-x/2}Al_{x/2}})0_3 + x\mathrm{MgO} \quad (1)$$

$$x/2\ \mathrm{Mg_2Al_2O_5} + (1-x/2)\mathrm{MgSiO_3} \rightarrow (\mathrm{Mg_{1-x/2}Al_{x/2}}) \times (\mathrm{Si_{1-x/2}Al_{x/2}})\mathrm{O_3} + x\mathrm{MgO} \quad (2)$$

$$(1-x)\mathrm{MgSiO_3} + x\mathrm{Al_2O_3} \rightarrow (\mathrm{Mg_{1-x}Al_x})(\mathrm{Si_{1-x}Al_x})\mathrm{O_3} \quad (3)$$

$$(1-x)\mathrm{MgSiO_{3Pv}} + (\mathrm{Mg_{1-x}Al_x})(\mathrm{Si_{1-x}Al_x})\mathrm{O_{3PPv}} \rightarrow (1-x)\mathrm{MgSiO_{3PPv}} + (\mathrm{Mg_{1-x}Al_x})\mathrm{O_{3Pv}} \quad (4)$$

Eqs. (1) and (2) represent the transformation (from left to right) from oxygen-vacancy (OVM) substitution to charge-coupled (CCM) substitution. MgO is considered to be in excess, as is probably the case in the Earth's lower mantle. We calculated the reaction enthalpy ΔH

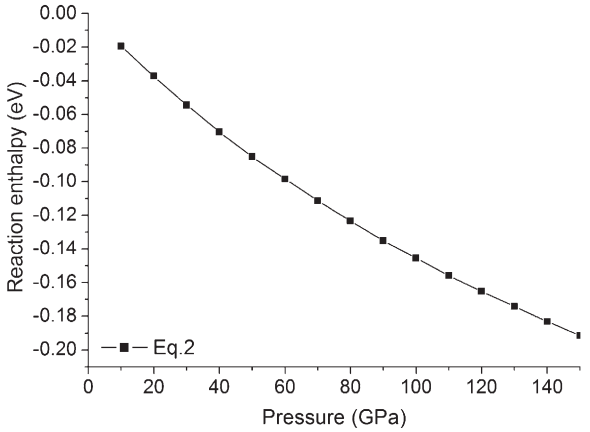

Fig. 5. Calculated enthalpy difference, ΔH, for the reaction in Eq. (2) as a function of pressure. Negative values suggest that normal post-perovskite is more favored than the more-compressible oxygen-vacancy-rich $Mg_2Al_2O_5$ in the Earth's lower mantle and the D″ layer.

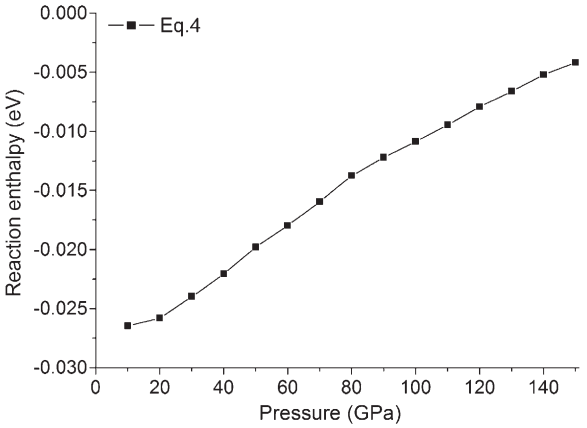

Fig. 6. Al–Al coupled substitution enthalpy difference between perovskite and post-perovskite. This reaction is shown in Eq. (4). Negative values indicate greater solubility of Al_2O_3 in perovskite.

as a function of pressure between 10 GPa and 150 GPa, the results are shown in Fig. 4 for Eq. (1) and Fig. 5 for Eq. (2). The reaction enthalpy ΔH is negative for both reactions at these pressures. This means that Al^{3+} ions should go into *PPv* through the CCM at all pressures up to 150 GPa. This is different from the case of *Pv*, where as suggested by Brodholt [28] the OVM could be favored below 30 GPa.

Eq. (3) presents the feasibility of the Al^{3+} ion substitution into *PPv* via CCM. In order to compare the stability of Al^{3+} in *Pv* and *PPv*, we calculated the differences between the reaction enthalpies ΔH for Eq. (3) between *Pv* and *PPv*. The result (reaction enthalpy of Eq. (4)) as a function of pressure is shown in Fig. 6 and demonstrates that Al strongly prefers to enter *Pv*, even though Al_2O_3 will adopt post-perovskite structure above 130 GPa [13–16]. Coupled [Fe^{3+}–Al^{3+}] substitutions in *Pv* [21–23] further enhance fractionation of Al into *Pv* [21]. The Al partition coefficient ($K = \exp(-\Delta H/K_b T)$) is $K = 4.25$ between *Pv* and *PPv* for the Fe-bearing system, $K = 2.67$ for Fe-free system at 120 GPa and 3000 K. The partition coefficient for Fe-free system obtained here is consistent with the previous work [19], where $K = 2.27$ was found at 120 GPa and 4000 K.

Fig. 7 shows the effect of incorporation of 3.125 mol % of Al_2O_3 on the *Pv*–*PPv* phase transition pressure for the most favorable substitution mechanism. The additional Al_2O_3 (6.25 mol% of Al^{3+}) slightly increases (~5 GPa) the transition pressure relative to pure $MgSiO_3$. This result is consistent with findings of Akber-Knutson et al [17], Caracas and Cohen [18] and Ono and Oganov [19].

4. Conclusions

We have performed large-scale density functional calculations to investigate in detail (1) the substitution mechanism of Al^{3+} ions in *PPv*, (2) the compressibility

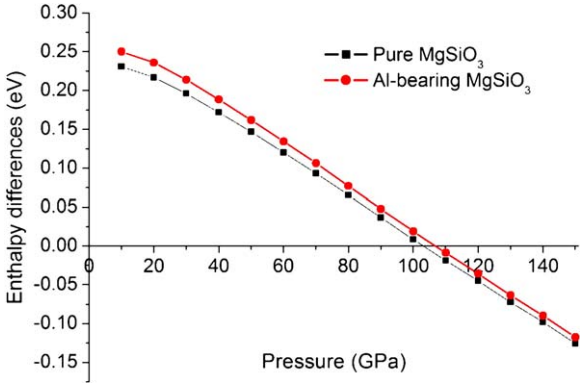

Fig. 7. Effect of chemical impurities 6.25 mol% Al^{3+} on the *Pv*–*PPv* phase transition pressure. From nearest CCM coupled *Pv* to the next nearest CCM2 coupled *PPv*.

of aluminous post-perovskite in the lower mantle, (3) the Al partitioning between *Pv* and *PPv*, and (4) the effect of Al_2O_3 on the *PPv* phase transition pressure. We considered 10 configurations, 5 for the OVM and 5 for the CCM, and an additional Si-free end-member $Mg_2Al_2O_5$, at various pressures spanning the range of the lower mantle, form 10 GPa to 150 GPa. These calculations show that CCM2, in which the next nearest pair of Mg^{2+} and Si^{4+} is replaced by two Al^{3+} ions, should be more favorable than other CCMs and OVMs throughout lower mantle pressures. This result is quite different from the Al substitution configuration in *Pv*, where the nearest pair configuration is most favorable, crystallographic reasons of this difference deserve a separate investigation. The calculated bulk moduli of the aluminous *PPv* are slightly lower than those of Al-free *PPv*. Al_2O_3 much easier goes into *Pv* than *PPv*, even though Al_2O_3 will adopt the *PPv* structure above 130 GPa. The incorporation of Al_2O_3 slightly increases the *PPv* phase transition pressure. As our previous work has shown the substitutions of Al^{3+} and Fe^{3+} are independent of each other in *PPv*, unlike in *Pv*. Therefore, the effects of these impurities on *PPv* can be decoupled and studied separately. While the effects of Al^{3+} are rather small for properties studied here, further theoretical and experimental work is needed to understand better the effects of Fe^{3+} impurities.

Acknowledgements

We gratefully acknowledge access to supercomputers at CSCS (Manno) and the HP Superdome of ETH Zürich. This work was supported by ETH Zurich (grant TH-32/04-3). FZH acknowledges Daniel Jung and Donat Adams for discussions.

References

[1] T. Lay, D.V. Helmberger, A shear velocity discontinuity in the lower mantle, Geophys. Res. Lett. 10 (1983) 63–66.
[2] T. Lay, Q. Williams, E.J. Garnero, The core–mantle boundary layer and deep Earth dynamics, Nature 392 (1998) 461–468.
[3] I. Sidorin, M. Gurnis, D.V. Helmberger, X. Ding, Interpreting D″ seismic structure using synthetic waveforms computed from dynamic models, Earth Planet. Sci. Lett. 163 (974) (1998) 31–41.
[4] I. Sidorin, M. Gurnis, D.V. Helmberger, Evidence for a ubiquitous seismic discontinuity at the base of the mantle, Science 286 (1999) 1326–1331.
[5] M. Panning, B. Romanowicz, Inferences of flow at the base of Earth's mantle based on seismic anisotropy, Science 33 (980) (2004) 351–353.
[6] M. Ishii, J. Tromp, Normal-mode and free-air gravity constraints on lateral variations in velocity and density of Earth's mantle, Science 285 (1999) 1231–1236.
[7] T. Irifune, Absence of an aluminous phase in the upper part of the Earth's lower mantle, Nature 370 (1994) 131–133.
[8] B.J. Wood, Phase transformations and partitioning relations in peridotite under lower mantle conditions, Earth Planet. Sci. Lett. 174 (2000) 341–354.
[9] M. Murakami, K. Hirose, K. Kawamura, N. Sata, Y. Ohishi, Post-perovskite phase transition in $MgSiO_3$, Science 307 (2004) 855–858.
[10] A.R. Oganov, S. Ono, Theoretical and experimental evidence for a post-perovskite phase of $MgSiO_3$ in Earth's D″ layer, Nature 430 (2004) 445–448.
[11] T. Iitaka, K. Hirose, K. Kawamura, M. Murakami, The elasticity of the $MgSiO_3$ post-perovskite phase in the Earth's lowermost mantle, Nature 430 (2004) 442–445.
[12] S. Ono, T. Kikegawa, Y. Ohishi, High-pressure phase transition of hematite, Fe_2O_3, J. Phys. Chem. Solids 65 (2004) 1527–1530.
[13] A.R. Oganov, S. Ono, The high-pressure phase of alumina and implications for Earth's D″ layer, Proc. Natl. Acad. Sci. U. S. A. 102 (2005) 10828–10831.
[14] R. Caracas, R.E. Cohen, Prediction of a new phase transition in Al_2O_3 at high pressures, Geophys. Res. Lett. 32 (2005) L06303.
[15] J. Tsuchiya, T. Tsuchiya, R.M. Wentzcovitch, Transition from the Rh_2O_3(II)-to-$CaIrO_3$ structure and the high-pressure–temperature phase diagram of alumina, Phys. Rev., B 72 (2005) 020103(R).
[16] S. Stackhouse, J.P. Brodholt, G.D. Price, High temperature elastic anisotropy of the perovskite and post-perovskite polymorphs of Al_2O_3, Geophys. Res. Lett. 32 (2005) L13305.
[17] S. Akber-Knutson, G. Steinle-Neumann, P.D. Asimow, Effect of Al on the sharpness of the $MgSiO_3$ perovskite to post-perovskite phase transition, Geophys. Res. Lett. 14 (2005) L14303.
[18] R. Caracas, R.E. Cohen, Effect of chemistry on the stability and elasticity of the perovskite and post-perovskite phases in the $MgSiO_3$–$FeSiO_3$–Al_2O_3 system and implications for the lowermost mantle, Geophys. Res. Lett. 32 (2005) L16310.
[19] S. Ono, A.R. Oganov, In situ observation of phase transition between perovskite and $CaIrO_3$-type phase in $MgSiO_3$ and pyrolitic mantle composition, Earth Planet. Sci. Lett. 236 (2005) 914–932.
[20] F. Zhang, A.R. Oganov, Theoretical evidence for the existence of iron metal and ferric iron-rich magnesium silicates in the lower mantle, Earth Planet. Sci. Lett. (submitted for publication).
[21] B.J. Wood, D.C. Rubie, The effect of alumina on the phase transformations at the 660-kilometer discontinuity from Fe–Mg partitioning experiments, Science 273 (1996) 1522–1524.
[22] S. Lauterbach, C.A. McCammon, P. van Aken, F. Langenhorst, F. Seifert, Mössbauer and ELNES spectroscopy of (Mg,Fe)(Si,Al)O_3 perovskite: a highly oxidised component of the lower mantle, Contrib. Mineral. Petrol. 138 (2000) 17–26.
[23] D.J. Frost, F. Langenhorst, The effect of Al_2O_3 on Fe–Mg partitioning between magnesiowüstite and magnesium silicate perovskite, Earth Planet. Sci. Lett. 199 (2002) 227–241.
[24] G. Kresse, J. Furthmüller, Efficiency of ab initio total-energy calculations for metals and semiconductors using a plane-wave basis set, Comput. Mater. Sci. 6 (1996) 15–50.
[25] J.P. Perdew, K. Burke, M. Ernzerhof, Generalized gradient approximation made simple, Phys. Rev. Lett. 77 (1996) 3865–3868.
[26] P.E. Blöchl, Projector augmented-wave method, Phys. Rev., B 50 (1994) 17953–17979.
[27] G. Kresse, D. Joubert, From ultrasoft pseudopotentials to the projector augmented-wave method, Phys. Rev., B 59 (1999) 1758–1775.

[28] J.P. Brodholt, Pressure-induced changes in the compression mechanism of aluminous perovskite in the Earth's mantle, Nature 407 (2000) 620–622.
[29] T. Yamamoto, D.A. Yuen, T. Ebisuzaki, Substitution mechanism of Al ions in $MgSiO_3$ perovskite under high pressure conditions from first-principles calculations, Earth Planet. Sci. Lett. 206 (2003) 617–625.
[30] A. Navrotsky, A lesson from ceramics, Science 284 (1999) 1788–1789.
[31] A.R. Oganov, G.D. Price, Ab initio thermodynamics of $MgSiO_3$ perovskite at high pressures and temperatures, J. Chem. Phys. 122 (2005) 124501.
[32] S. Speziale, C.-S. Zha, S. Duffy, J. Hemley, K. Mao, Quasi-hydrostatic compression of magnesium oxide to 52 GPa: implications for the pressure–volume–temperature equation of state, J. Geophys. Res. 106 (2001) 515–528.